0022-3565/09/3283-715–722$20.00
THE JOURNAL OF PHARMACOLOGY AND EXPERIMENTAL THERAPEUTICS
JPET 328:715–722, 2009

Vol. 328, No. 3
147330/3439487
Printed in U.S.A.

Microtubule Binding and Disruption and Induction of Premature Senescence by Disorazole C_1 [S]

Marni Brisson Tierno, Carolyn A. Kitchens, Bethany Petrik, Thomas H. Graham, Peter Wipf, Fengfeng L. Xu, William S. Saunders, Brianne S. Raccor, Raghavan Balachandran, Billy W. Day, Jane R. Stout, Claire E. Walczak, Alexander P. Ducruet, Celeste E. Reese, and John S. Lazo

Drug Discovery Institute (M.B.T., C.A.K., B.P., P.W., B.W.D., A.P.D., C.E.R., J.S.L.), Departments of Pharmacology and Chemical Biology (M.B.T., C.A.K., A.P.D., J.S.L.), Chemistry (T.H.G., P.W.), Biological Sciences (F.L.X., W.S.S.), and Pharmaceutical Sciences (B.S.R., R.B., B.W.D.), and Center for Chemical Methodologies and Library Development (P.W.), University of Pittsburgh, Pittsburgh, Pennsylvania; and Medical Sciences Program, Indiana University, Bloomington, Indiana (J.R.S., C.E.W.)

Received October 10, 2008; accepted December 8, 2008

ABSTRACT

Disorazoles comprise a family of 29 macrocyclic polyketides isolated from the fermentation broth of the myxobacterium *Sorangium cellulosum*. The major fermentation product, disorazole A_1, was found previously to irreversibly bind to tubulin and to have potent cytotoxic activity against tumor cells, possibly because of its highly electrophilic epoxide moiety. To test this hypothesis, we synthesized the epoxide-free disorazole C_1 and found it retained potent antiproliferative activity against tumor cells, causing prominent G_2/M phase arrest and inhibition of in vitro tubulin polymerization. Furthermore, disorazole C_1 produced disorganized microtubules at interphase, misaligned chromosomes during mitosis, apoptosis, and premature senescence in the surviving cell populations. Using a tubulin polymerization assay, we found disorazole C_1 inhibited purified bovine tubulin polymerization, with an IC_{50} of 11.8 $\pm$ 0.4 μM, and inhibited [^{3}H]vinblastine binding noncompetitively, with a K_i of 4.5 $\pm$ 0.6 μM. We also found noncompetitive inhibition of [^{3}H]dolastatin 10 binding by disorazole C_1, with a K_i of 10.6 $\pm$ 1.5 μM, indicating that disorazole C_1 bound tubulin uniquely among known antimitotic agents. Disorazole C_1 could be a valuable chemical probe for studying the process of mitotic spindle disruption and its relationship to premature senescence.

Natural products have provided a plethora of pharmacologically useful drugs and chemical probes. The disorazole polyene macrodiolides were first isolated from the myxobacterium *Sorangium cellulosum* in 1994 and characterized to have significant antifungal activity with no antibacterial activity (Jansen et al., 1994). Initial biochemical and pharmacological studies were restricted to the major fermentation product, disorazole A_1 (Fig. 1), which blocks cell proliferation, causes G_2/M phase arrest and loss of microtubules, and induces apoptosis. Moreover, it blocks in vitro polymerization of tubulin (Elnakady et al., 2004; Kopp et al., 2005). Disorazole A_1 contains a highly electrophilic divinyl oxirane moiety that we hypothesized might mediate the mitotic arrest and inhibition of tubulin polymerization through covalent binding to tubulin (Wipf et al., 2006). The highly electrophilic divinyl oxirane of disorazole A_1 is generally not viewed as a therapeutically desirable moiety; therefore, we synthesized the rare family member disorazole C_1 (Fig. 1), which is devoid of reactive groups. It is remarkable that disorazole C_1 retained antimitotic activity (Wipf and Graham, 2004; Wipf et al., 2006). Structural analogs suggested that the functional group array of disorazole C_1 and its three-dimensional conformation were critical for biological activity, but little is known about its mechanism of action. In the current comprehensive report, we demonstrate that disorazole C_1 has potent antiproliferative activity against a wide variety of human tumor cells, disrupts cellular microtubule integrity, blocks tubulin polymerization in vitro, binds tubulin in a unique manner, and causes apoptosis and premature cellular senes-

This work was supported by the National Institutes of Health [Grants CA078039 and CA097190; SPORE in Head and Neck Cancer]; the Fiske Drug Discovery Fund; and the METACyt Initiative of Indiana University [partially funded through a grant from the Lilly Endowment, Inc.].
Article, publication date, and citation information can be found at http://jpet.aspetjournals.org.
doi:10.1124/jpet.108.147330.
[S] The online version of this article (available at http://jpet.aspetjournals.org) contains supplemental material.

ABBREVIATIONS: DMSO, dimethyl sulfoxide; TUNEL, terminal deoxynucleotidyl transferase dUTP nick-end labeling; BrdU, 5-bromo-2′-deoxyuridine; JG-03-14, 2,4-dibromo-5-carbethoxyoy-3-(3,4-dimethyoxyphenyl)pyrrole.

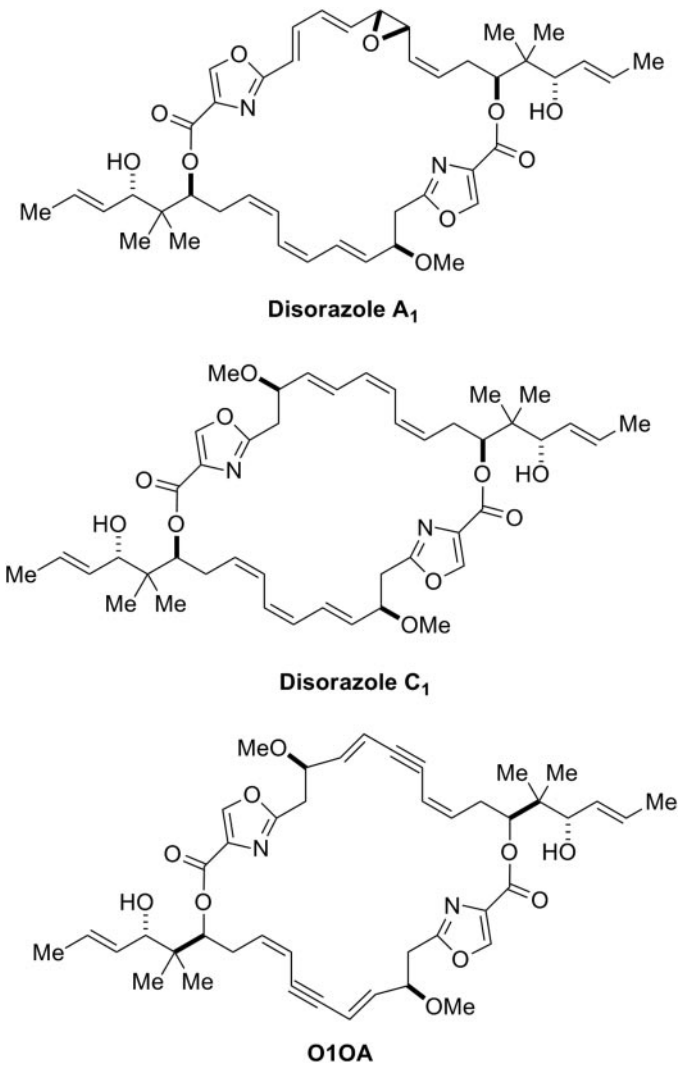

Fig. 1. Chemical structures of disorazoles.

cence, all attributes associated with a promising anticancer agent.

Materials and Methods

Cell Culture Reagents and Proliferation Assays. Cells were cultured in the following media supplemented with 10% fetal bovine serum (VWR, West Chester, PA): PtK2 rat kangaroo kidney epithelial cells in minimal essential medium-α; head and neck squamous cell carcinoma cell lines in Dulbecco's modified Eagle's medium; A549 and WI-38 fibroblasts in basal medium Eagle; UPCI:SCC103 in minimal essential medium; and MDA-MB-231, PC-3, and 2008 in RPMI; and HCT116 in McCoy's 5A. Unless otherwise indicated, all media, sera, and supplements were obtained from Invitrogen (Carlsbad, CA), and other reagents were from Sigma-Aldrich (St. Louis, MO).

Inhibition of growth was determined spectrophotometrically with 3-(4,5-dimethylthiazol-2-yl)-2,5-diphenyltetrazolium bromide or by measuring fluorescence in live cells using an alamar blue-based assay (Promega, Madison, WI). Alternatively, in some studies, we fixed cells in 3.7% formaldehyde and stained nuclei with 2 μg/ml Hoechst 33342 dye to quantify cells using an ArrayScan VTi (Thermo Fisher Scientific, Waltham, MA). The 50% growth-inhibitory concentrations (IC_{50}) of test agents were calculated after a 72-h incubation. For reversibility studies, we treated A549 cells for 1 h with vehicle, 10 nM disorazole C_1, or 1 μM nocodazole. Cells were either continuously exposed to compound in complete medium or briefly (1 h) exposed to a compound, which was removed by washing three times with complete medium. Live cells were counted by trypan blue exclusion and normalized to control cells. For studies with quiescent cell studies, confluent WI-38 cells were treated for 72 h with either DMSO or disorazole C_1.

Immunofluorescence Detection of Microtubules. PtK2 cells (3×10^4 cells/35 mm well) were plated 48 h before treatment. Cells were rinsed twice to remove antibiotics and incubated for 24 h with compounds diluted in antibiotic-free growth medium. Cells were processed to visualize microtubules and DNA, and digital images were collected and manipulated as described previously (Stout et al., 2006). A549 cells were plated on coverslips in six-well plates for 24 h before compound treatment, fixed in 3.7% paraformaldehyde, and incubated in 0.1% Triton X-100 at 4°C for 7 min. A 1% solution of bovine serum albumin in phosphate-buffered saline plus 0.1% Tween was used as the blocking buffer. Microtubules were visualized using an anti-α-tubulin mouse monoclonal antibody (Abcam Inc., Cambridge, MA) with goat-anti-mouse Alexa Fluor488 (Invitrogen) secondary antibody diluted in 1% bovine serum albumin/phosphate-buffered saline plus 0.1% Tween. Nuclei were visualized with the fluorescent dye 4,6-diamidino-2-phenylindole and an Olympus BX60 epifluorescence microscope (Olympus, Tokyo, Japan). Images were taken using a Hamamatsu Argus-20 CCD camera and image processor (Hamamatsu Corporation, Bridgewater, NJ).

Radioligand Binding and Inhibition of Tubulin Assembly. Tubulin was isolated from bovine brain as described previously (Hamel and Lin, 1984). [^{3}H]Vinblastine (specific activity, 61–315 mCi/mmol) and Sephadex G-50 were from GE Healthcare (Chalfont St. Giles, UK). Handee centrifuge columns and the bicinchoninic acid protein assay kit were from Pierce Chemical (Rockford, IL). [^{3}H]Dolastatin 10 (specific activity, 26–133 mCi/mmol), dolastatin 10, and paclitaxel were from the Drug Synthesis and Chemistry Branch at the National Cancer Institute (Rockville, MD). Radiolabeled ligand binding to tubulin was measured by centrifugal gel filtration and scintillation spectrometry as described previously (Bai et al., 1995b), with minor modifications (Wang et al., 2007). The average stoichiometry of binding in the control reaction mixture was 0.63 mol [^{3}H]vinblastine or [^{3}H]dolastatin 10/mol of tubulin. For the tubulin assembly studies, we used homogeneous bovine brain tubulin (10 μM) and previously described methods (Wang et al., 2007).

Apoptosis and Senescence Assays. A549 cell were analyzed for apoptosis using a commercially available fluorescein terminal deoxynucleotidyl transferase dUTP nick-end labeling (TUNEL) method with fluorescence microscopy as described by the manufacturer (Roche In Situ Cell Death Kit; Roche Diagnostics, Indianapolis, IN). For senescence measurements, A549 cells (3.5×10^5 cells/well) were plated 24 h before treatment with DMSO vehicle or test compounds for 1 to 7 days. For 7-day treatments, individual wells were split on day 3 or 4 to avoid the cultures reaching confluence. β-Galactosidase staining was performed as described previously (Dimri et al., 1995) and quantified both by visual counting by a naive observer or by acquiring images with the bright-field module on an ArrayScan VTI and using the Cellomics Compartmental Analysis V3 Bioapplication (Cellomics, Inc., Pittsburgh, PA) to define cells with positive β-galactosidase staining (mean of 20 acquired fields/well). For BrdU incorporation, A549 cells were pretreated in thymidine-free medium, incubated for 6 h with BrdU, and visualized using a cell proliferation kit (GE Healthcare). BrdU images were acquired (20 fields/well) with an ArrayScan VTi and analyzed using the Cellomics Compartmental Analysis V3 Bioapplication[1] to determine the percentage of cells with fluorescence greater than the set threshold and to quantify BrdU-positive cells. For Western blotting, A549 cells were treated with

[1] M. B. Tierno, B. Petrik, D. Nickischer, and P. Johnston, Application Note LC01612000, Thermo Scientific, Pittsburgh, PA. http://www.cellomics.com/content/menu/Compartmental_Analysis_AS/

compounds for 7 days as stated above followed by cell harvesting in ice-cold lysis buffer (50 mM Tris, pH 7.6, containing 150 mM NaCl, 1 mM EDTA, 0.1% SDS, and 1% Triton X-100) supplemented with protease and phosphatase inhibitors. Protein concentrations in cell lysates were determined with the BCA protein assay kit (Promega). Individual proteins were detected by standard Western blotting methods with the following antibodies: p53, pRb, phospho-Rb (Ser780), γH2AX, and GAPDH antibodies (Cell Signaling Technology Inc., Danvers, MA); p21 antibody (EMD Biosciences, San Diego); vinculin (Santa Cruz Biotechnology, Inc., Santa Cruz, CA); cyclin D antibody (BD Biosciences, San Jose, CA). Discodermolide was obtained from Novartis (Basel, Switzerland), and disorazole A1 was from Æterna Zentaris GmbH (Frankfurt, Germany).

Results

Disorazole C_1 is a Potent Inhibitor of Cell Proliferation, Interferes with Tubulin Polymerization, and Binds to Tubulin. As an extension of our previous study with HeLa cells (Wipf et al., 2006), we examined the growth-inhibitory activity of disorazole C_1 using 11 other human tumor carcinoma cell lines (Table 1). Disorazole C_1 was remarkably potent, with an average 50% growth-inhibitory concentration (IC_{50}) of 1.7 ± 0.6 nM (S.E.M.). Head and neck cancer cell lines were particularly sensitive to disorazole C_1, with an average IC_{50} value of 358 ± 56 pM. The p53 wild-type HCT116 cells exhibited similar sensitivity to disorazole C_1 compared with the p53 null MDA-MB-231 cells. When quiescent WI-38 fibroblasts were exposed to disorazole C_1 for 72 h, we observed no change in cell number or morphology. In contrast, proliferating WI-38 cells were sensitive to disorazole C_1, indicating that active cell division was important for the cytotoxic effects of disorazole C_1.

Disorazole A_1 was reported previously to inhibit tubulin polymerization in vitro at substoichiometric concentrations and block cell proliferation at the G_2/M phase (Elnakady et al., 2004). We previously observed that disorazole C_1 caused G_2/M phase arrest with HeLa cells (Wipf et al., 2006). As illustrated in Fig. 2A, disorazole C_1 clearly disrupted GTP-mediated tubulin assembly in a concentration-dependent manner, with an IC_{50} of 11.8 ± 0.4 μM (Fig. 2A), indicating a compound/tubulin stoichiometry of approximately 1:1.

We next probed the ability of disorazole C_1 to inhibit the binding of [^{3}H]vinblastine or [^{3}H]dolastatin 10 to purified tubulin as described previously (Bai et al., 1995b) (Fig. 2, B and C). As illustrated by the intersecting lines in the Hanes-Woolf plot (Fig. 2B), disorazole C_1 inhibited [^{3}H]vinblastine binding in an noncompetitive manner, with a K_i of 4.5 ± 0.6 μM. With this linear transformation, the lines would be parallel if the inhibition was competitive. Dolastatin 10 binds at the depsipeptide binding site on tubulin, which overlaps with the vinca alkaloid binding site (Bai et al., 1995a,b). It is interesting that we also found noncompetitive inhibition of [^{3}H]dolastatin 10 binding by disorazole C_1, with a K_i of 10.6 ± 1.5 μM, suggesting that disorazole C_1 might bind tubulin uniquely among known antimitotic agents.

We next treated A549 cells with IC_{50} concentrations of disorazole C_1 or vinblastine and visualized microtubule integrity by immunofluorescence microscopy (Fig. 3). Compared with vehicle control, disorazole C_1 disrupted microtubules as early as 24 h (Fig. 3b) with complete disruption within 72 h (Fig. 3c). Even within 1 h, disorazole C_1 (2 nM, Fig. 3f; 10 nM, Fig. 3g; 20 nM, Fig. 3h) and 20 nM vinblastine (Fig. 3i) caused a dissolution of microtubules.

To further assess the effects of disorazole C_1 on microtubules at interphase and mitosis, we examined PtK2 rat kangaroo kidney epithelial cells, which are widely used to study antimitotics because they have a flat morphology and large chromosomes, allowing greater visualization. PtK2 cells were treated for 24 h in the presence of disorazole C_1 (5, 25, or 100 nM) or the inactive but structurally closely related analog O1OA (Fig. 1). O1OA had no effect on microtubules at interphase or mitosis, where chromosomes aligned normally along the metaphase plate (Fig. 4). In contrast, disorazole C_1 completely disrupted microtubules at both concentrations. At mitosis, complete misalignment of chromosomes was evident, as were multipolar spindles and dispersed chromosomes with no attached microtubules. These results, in combination with the data described in Fig. 3, confirmed that disorazole C_1 treatment had a dramatic effect on cellular microtubules, causing disruption of normal mitotic processes.

We next determined the durability of the growth-inhibitory effects of disorazole C_1. A549 cells were treated for 1 h with 10 nM disorazole C_1, 1 μM nocodazole, or DMSO vehicle and

TABLE 1

Growth inhibition with microtubule-disrupting agents

Human cells were plated in 96-well plates, allowed to attach for 24 h, and treated for 72 h with DMSO or a range of concentrations of test agents. Cell number was determined spectrophotometrically at 570 nm minus absorbance at 690 nm after exposure to 3-(4,5-dimethylthiazol-2-yl)-2,5-diphenyltetrazolium or by measuring fluorescence (excitation, 560; emission, 590) in live cells using the Cell Titer Blue Assay (Promega).

Cell Line	Description	IC_{50} ± S.E.M.[a]		
		Disorazole C_1	Vincristine	Vinblastine
			nM	
A549	Lung carcinoma	2.21 ± 0.23	21.62 ± 2.68	1.52 ± 0.09
PC-3	Prostate adenocarcinoma carcinoma	1.57 ± 0.10	4.68 ± 0.29	0.86 ± 0.08
MDA-MB-231	Breast epithelial adenocarcinoma	3.53 ± 0.19	7.16 ± 0.37	1.34 ± 0.21
2008	Ovarian carcinoma	1.91 ± 0.23	21.81 ± 2.92	2.24 ± 0.16
HCT116	Colorectal carcinoma	1.09 ± 0.41	5.62 ± 0.33	1.40 ± 0.07
UPCI:SCC104	Oral squamous carcinoma	6.87 ± 0.54	2.98 ± 0.22	1.13 ± 0.18
PCI 15A	Head and neck squamous carcinoma	0.26 ± 0.03	0.41 ± 0.04	1.86 ± 0.14
PCI 15B	Head and neck squamous carcinoma	0.34 ± 0.03	0.94 ± 0.20	1.81 ± 0.27
PCI 37A	Head and neck squamous carcinoma	0.53 ± 0.07	0.66 ± 0.06	2.51 ± 0.06
PCI 37B	Head and neck squamous carcinoma	0.26 ± 0.02	0.49 ± 0.05	3.58 ± 0.45
UMSCC22A	Head and neck squamous carcinoma	0.40 ± 0.06	1.45 ± 0.24	3.27 ± 0.70
WI-38 confluent	Fibroblasts	>100	ND	>100
WI-38 proliferating	Fibroblasts	1.74 ± 0.78	8.58 ± 0.78	1.54 ± 0.13

[a] IC_{50} values are mean of eight determinations.

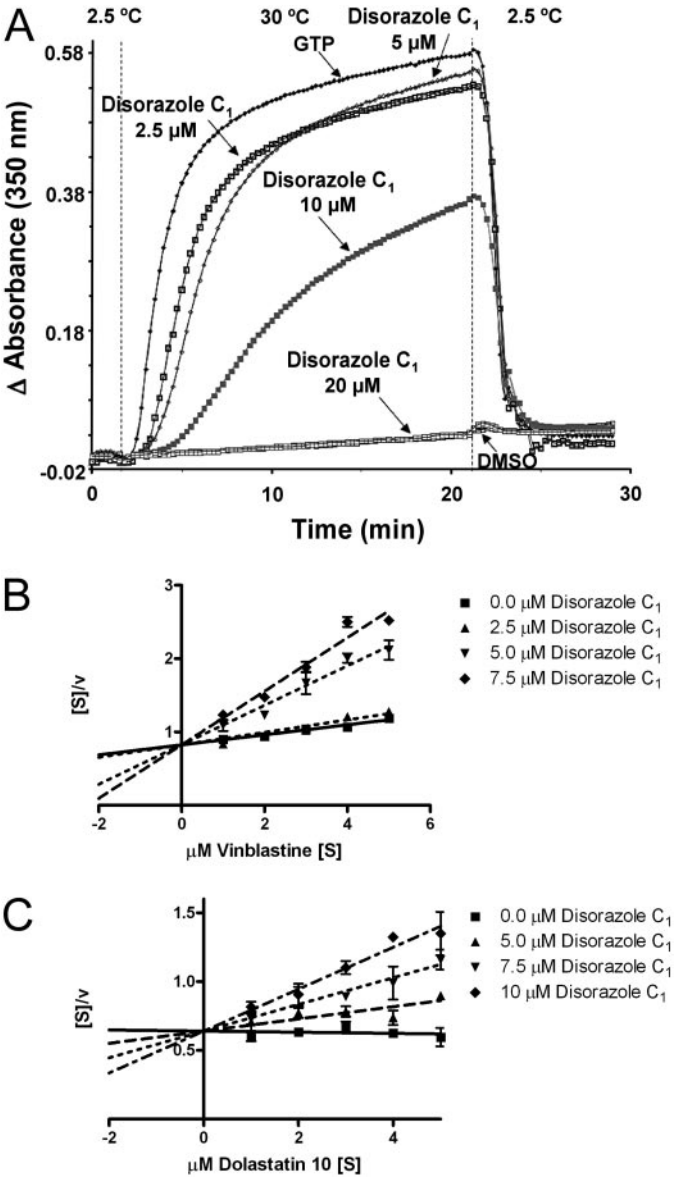

Fig. 2. Disorazole C_1 disrupts microtubule assembly and binds to tubulin in vitro. A, bovine brain tubulin was preincubated with disorazole C_1 or vehicle and monosodium glutamate for 15 min at 30°C. The reaction mixture was cooled to 0°C, GTP was added, reaction mixtures were transferred to cuvettes, held at 2.5°C in a spectrophotometer, and absorbance (turbidity) was read at 350 nm. After a baseline was established, the temperature was raised to 30°C (~1 min). After 20 min, the temperature was returned to 2.5°C. GTP alone (no test compound) was assigned as 100% assembly (positive control) and DMSO alone (no test compound, no GTP) as 0% assembly (negative control). Hanes-Woolf plot of disorazole C_1 inhibition of [^{3}H]vinblastine (B) or [^{3}H]dolastatin 10 (C) binding to 10 μM bovine brain tubulin. The mixtures were incubated for 30 min at room temperature and bound versus free radiolabeled ligand was separated using Sephadex G-50 columns. The amount of radiolabeled ligand bound to tubulin was determined using scintillation spectrometry. The substrate concentration ([S]) is indicated on the abscissa and the ratio of the substrate concentration to the reaction velocity ([v]) indicated on the ordinate.

were maintained in medium containing compound (contin) or washed and maintained in medium lacking compound (wash) and incubated for 1 to 144 h (Fig. 5A). The cytotoxic effects of nocodazole, a reversible inhibitor of mitosis, were completely reversed with compound washout. In contrast, cell viability continued to decline during the 72 h in cultures exposed

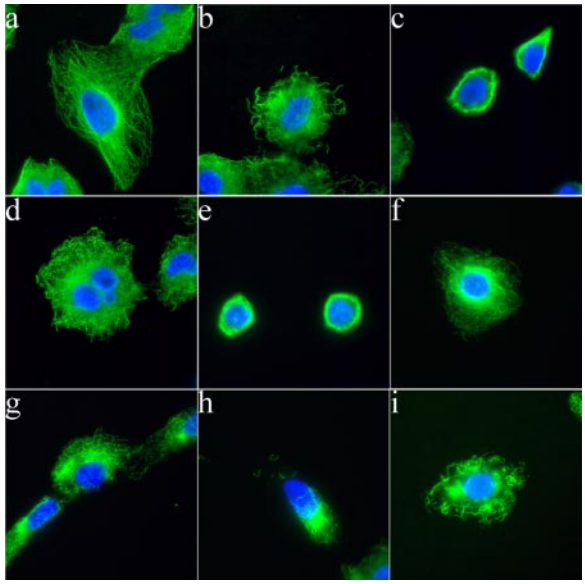

Fig. 3. Disorazole C_1 disrupts microtubules in vivo. Microtubules in A549 cells were partially disrupted after disorazole treatment at 2 nM for 24 h (b) and more completely at 72 h (c) compared with DMSO vehicle control (a). The disruption was similar to that seen with 2 nM vinblastine treatment at 24 h (d) and 72 h (e). A concentration response effect on microtubules after a 1-h treatment was observed with 2 nM (f), 10 nM (g), and 20 nM (h) disorazole C_1, similar to 20 nM vinblastine (i). With both compounds, apparent tubulin aggregation was observed at higher concentrations (h and i). Cells were fixed and stained with anti-α-tubulin antibody to visualize microtubules (green) and 4,6-diamidino-2-phenylindole to visualize nuclei (blue).

briefly (1 h) or continuously to 10 nM disorazole C_1. The number of surviving cell remained relatively constant between 72 and 144 h, suggesting growth arrest and possible senescence. A microscopic analysis of microtubule integrity

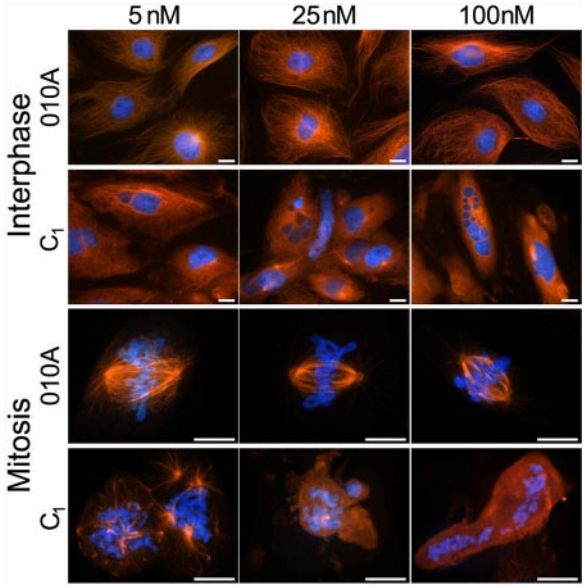

Fig. 4. Disorazole C_1 disrupts microtubules at interphase and metaphase. Mammalian PtK2 cells were treated with the indicated concentrations of either O1OA (inactive analog of disorazole C_1) or disorazole C_1 for 24 h at 37°C. Cells were fixed and stained with anti-α-tubulin antibody to visualize microtubules (red) and Hoechst 33342 to visualize chromosomes (blue). All images were collected with a Nikon E600 microscope (Nikon, Tokyo, Japan) equipped with a Roper CoolSnap HQ digital camera (Roper Scientific, Trenton, NJ) at 40× (interphase) or 100× (mitotic spindles) objectives. Top, interphase; bottom, mitosis. Bars, 10 μm.

also suggested the disorazole C_1-mediated microtubule disruption was not readily reversible. Furthermore, the IC_{50} values for cells treated for 1 h or 7 days were similar (2.2 versus 1.5 nM). These growth-inhibitory results were consistent with a previous report using disorazole A_1, in which the cytotoxic effects were prolonged (Elnakady et al., 2004). Disorazole C_1 at 10 nM caused some apoptosis in A549 cells (Fig. 5B), although it was much less effective than what has been reported for disorazole A_1 (Elnakady et al., 2004). Thus, treatment of A549 cells with 2 nM disorazole C_1 for 24 or 48 h caused no significant apoptosis as detected by a TUNEL assay, although treatment with 10 nM for 48 h did cause detectable apoptosis (Fig. 5B). These results indicate that the highly reactive vinyl oxirane subunit in disorazole A_1 was dispensable for the prolonged cytotoxicity caused by the disorazole family members.

Disorazole C_1 Induces Premature Senescence. Because drug-resistant cells have been so valuable in understanding the mechanism of action of new small molecules, we attempted to generate A549 cells that were resistant to disorazole C_1 using chronic exposure to increasing compound concentrations in culture. Although our initial efforts were unsuccessful, when we examined the population that survived a 1-week exposure, we observed cells with an enlarged, flattened morphology. These cells ceased to divide but remained viable for >50 days in the presence or absence of disorazole C_1. We tested whether or not these cells entered premature senescence using a classic β-galactosidase staining procedure at pH 6.0 after treatment of A549 cells for 7 days with 1 to 10 nM disorazole C_1 (Fig. 6). Cells treated with DMSO or the inactive O1OA analog displayed only a few sparse β-galactosidase-positive cells, whereas the positive control, doxorubicin, showed abundant β-galactosidase staining at the IC_{50} concentration of 50 nM. Cells treated with an IC_{50} concentration of discodermolide also displayed high levels of β-galactosidase-positive cells, whereas an equipotent growth-inhibitory concentration of vinblastine had no effect consistent with previous results (Chang et al., 1999; Klein et al., 2005). Disorazole C_1 treatment resulted in positive β-galactosidase staining even at concentrations below the growth IC_{50} (1 nM). The percentage of β-galactosidase-positive cells with disorazole C_1 treatment was comparable with that seen with doxorubicin. Disorazole C_1 also produced positive β-galactosidase human colon cancer (HCT116), lung cancer (H1299), and oral squamous carcinoma (UPCI:SCC103) cells, but not PC-3 prostate cancer cells (data not shown).

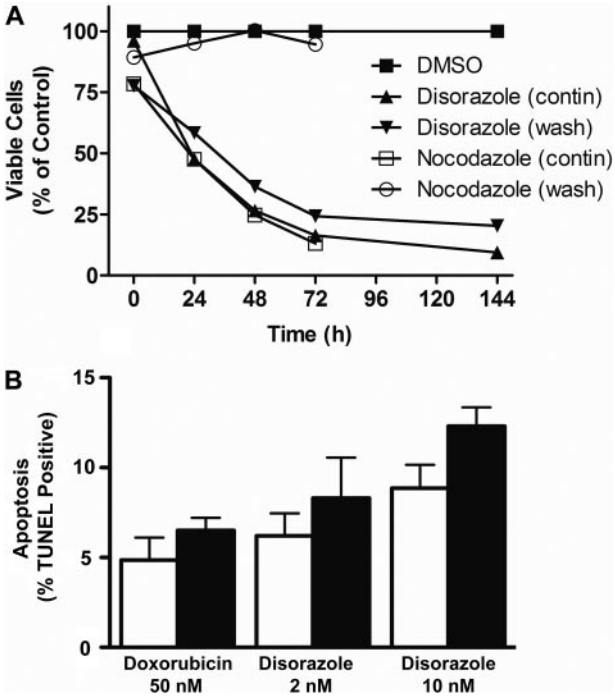

Fig. 5. Disorazole C_1 causes irreversible growth inhibition. A549 cells were treated for 1 h with 10 nM disorazole C_1, 1 μM nocodazolem, or DMSO vehicle followed by either washout of compound (wash) or continuous exposure to compound (contin) for 1, 24, 48, 72, and 144 h. Live cells were counted by trypan blue exclusion. The number of viable cells (trypan blue negative) is graphed as the percentage of viable cells per milliliter normalized to the DMSO control. Data are representative of two independent experiments. B, A549 cells were incubated with doxorubicin (50 nM) or disorazole C_1 (2 or 10 nM) for 24 (open bars) or 48 (black bars) h, and apoptosis was determined with a TUNEL assay. $n = 3$; bars, S.E.M.

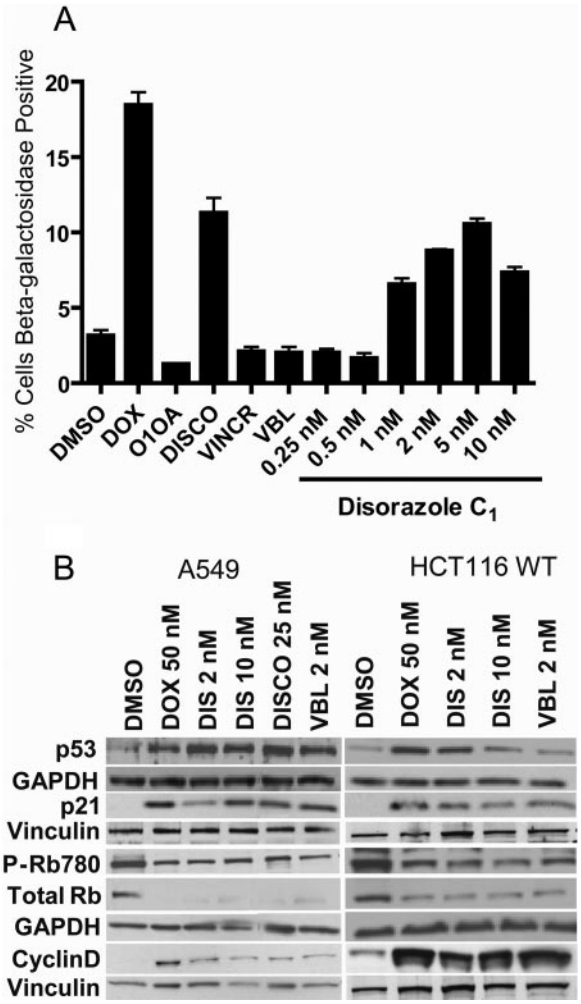

Fig. 6. Disorazole C_1 causes premature senescence. A, A549 cells were treated for 7 days with disorazole C_1, IC_{50} concentrations of discodermolide (DISCO; 25 nM), vincristine (VINCR; 20 nM), or vinblastine (VBL; 2 nM), followed by β-galactosidase staining, which was quantified using the bright-field module and compartmental bioapplication analysis on the ArrayScan VTI with values representative of at least two independent experiments. Doxorubicin (DOX; 50 nM) was used as a positive control for senescence, whereas DMSO vehicle and the inactive analog O1OA (10 nM) were used as negative controls. B, A549 and HCT116 cells were treated for 7 days, and cell lysates were probed by Western blot analysis of protein markers of senescence. GAPDH and vinculin, which were used as loading controls, are located directly below the examined protein lanes.

Alterations in the protein expression profiles of some of the classic markers of premature senescence also supported the hypothesis that these metabolically active, nondividing cells had undergone premature senescence. A549 and HCT116 cells were treated for 7 days with concentrations of 50 nM doxorubicin, 2 nM disorazole C1, 25 nM discodermolide, or 2 nM vinblastine that had equivalent growth inhibition. Cells were lysed, protein was isolated, and the protein expression was determined by Western blotting (Fig. 6B). All compounds increased the levels of cyclin dependent kinase inhibitor p21 and cyclin D. Lower levels of Ser780 phosphorylated pRb and total pRb levels were also observed as expected for cells undergoing cell cycle arrest and premature senescence. Vinblastine (2 nM) also induced p53, p21, Rb, and cyclin D consistent with cell cycle arrest and senescence, although little β-galactosidase staining was observed (Figs. 6 and 7).

Further documenting the role of microtubule disruption in premature senescence, we observed DNA synthesis as measured by BrdU incorporation was inhibited by 67% in A549 cells treated for 1 day with IC_{50} concentration of disorazole C_1 (2 nM), which was equivalent to that seen with the 50% growth-inhibitory concentration of doxorubicin (50 nM) (Supplemental Fig. 1; Supplemental Table 1). In contrast, almost all cells incorporated BrdU after treatment with the inactive analog O1OA, vinblastine, discodermolide, or DMSO vehicle control, indicating actively dividing cells. By 7 days, almost no cells were actively dividing after treatment with doxorubicin, discodermolide, or disorazole C_1 (≥0.5 nM) (Supplemental Fig. 1; Supplemental Table 1). Some decrease in BrdU-positive cells was seen after a week of treatment with either 10 nM O1OA or 2 nM vinblastine. We also excluded the possibility that the induction of premature senescence was the product of double-strand DNA breaks because we did not detect an increase in Ser139 phosphorylation of γH2AX after treatment with either disorazole C_1 or vinblastine (Supplemental Fig. 2). These results, in combination with the positive β-galactosidase staining and changes in cell cycle protein markers, indicate that disorazole C_1 could induce premature senescence in some human tumor cells.

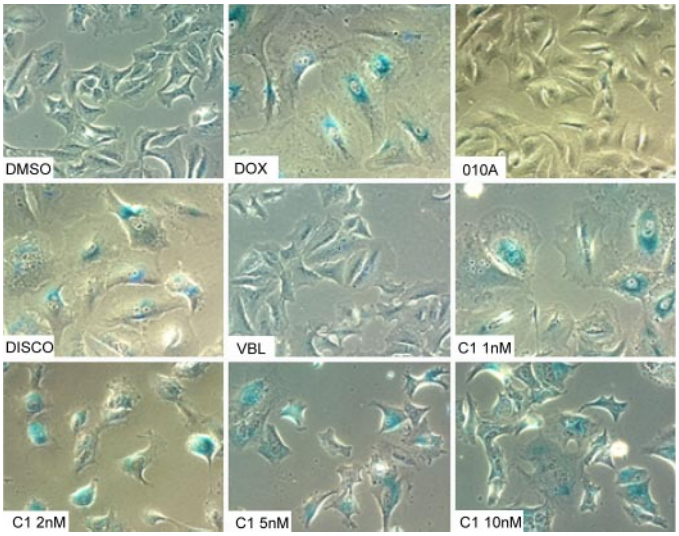

Fig. 7. Disorazole C_1 causes premature senescence. A549 cells were treated for 7 days with vehicle (DMSO), doxorubicin (DOX; 50 nM), the inactive analog 010A (10 nM), discodermolide (DISCO; 25 nM) vinblastine (VBL; 2 nM), or disorazole C_1 (C_1, 1–10 nM) followed by β-galactosidase staining.

Discussion

The highly electrophilic divinyl oxirane moiety of disorazole A_1 has been an attractive candidate mediator for the inhibition of tubulin polymerization, and our results indicate that at least some of the pharmacological activity of the disorazole family resides in other aspect of the disorazole pharmacophore. The disorazole C_1 concentration required to inhibit tubulin polymerization by 50% in vitro (namely, 11.8 μM) was approximately an order of magnitude higher than the IC_{50} values reported for disorazole A_1 (1.8 μM) using a similar assay (Elnakady et al., 2004). Our in vitro tubulin binding studies indicated that disorazole C_1 had a unique direct tubulin binding interaction, possibly binding at or near a site typically occupied by vinblastine and dolastatin 10. However, we could not rule out the possibility that disorazole C_1 bound to a completely unrelated site on tubulin, instigating a conformational change that allosterically interferes with vinblastine and dolastatin 10 binding. Further studies are needed to determine the exact binding domain of disorazole C_1 on tubulin. These results indicate disorazole C_1, like disorazole A_1 (Elnakady et al., 2004), inhibited tubulin polymerization in the absence of abundant microtubule-associated proteins.

Disorazole C_1 prevented proper assembly of microtubules within cells. The disorazole C_1 concentration required to inhibit tubulin polymerization by 50% in vitro would be expected to be higher because the concentration of purified tubulin (10 μM) used in the in vitro reactions was intentionally high to permit robust detection. Moreover, it is now recognized that most effective anticancer drugs affect microtubule depolymerization or polymerization at much lower concentrations than required for in vitro studies (Jordan and Wilson, 2004). The lower concentration of disorazole C_1 or A_1 required to disrupt cellular proliferation probably reflected the need to affect only a small fraction of the tubulin/microtubule dynamics to block the cell division machinery. The breakdown of microtubules was seen as early as 15 min after a 5 nM disorazole C_1 treatment, with complete absence of cells with visible microtubules within 4 h (data not shown). We speculate that the long-lived disorazole C_1 cytotoxicity might be because of misalignment of chromosomes at the metaphase plate, consistent with the G_2/M arrest and increase in mitotic index that we described previously (Wipf et al., 2006). All of these data indicated that disorazole C_1 was a potent, cytotoxic, microtubule destabilizer that prevents normal cell division. Nonetheless, the previously reported IC_{50} values for growth inhibition with disorazole A_1 suggest that it is even more potent than disorazole C_1, probably because of the highly reactive divinyl oxirane moiety. In preliminary growth inhibition studies with HeLa cells, we observed an IC_{50} of 47 pM for disorazole A_1 compared with an IC_{50} of 219 pM for disorazole C_1. It remains to be determined whether disorazole C_1 has a better therapeutic potential compared with the more potent disorazole A_1.

Proliferating cells that are subjected to significant harmful stress rapidly exit the cell cycle through several concurrent failsafe "checkpoint" mechanisms enabling DNA repair and suppressing possible tumorigenesis. If these cell cycle checkpoints are deficient because of the presence of mutations or overwhelming damage, cells generally engage in apoptosis or senescence. Senescence is defined as permanent cell-cycle

arrest preventing proliferation but permitting metabolic activity. Senescent cells have an enlarged, flattened morphology with an increased cytoplasmic area, increased granularity, extensive cytoplasmic vacuoles, and multinucleation (Schmitt, 2007). There currently is no single accepted biochemical defining marker for the senescence phenotype, although perinuclear lysosomal presence of β-galactosidase is often considered to be a senescence characteristic (Dimri et al., 1995). In addition, senescent cells do not synthesize DNA and therefore display decreased BrdU uptake. Cells undergoing senescence show changes in the expression of genes involved in tumor suppression, cell cycle progression, mitosis, and DNA replication. Thus, the tumor suppressor protein p53, which up-regulates the cyclin-dependent kinase inhibitors p21 and p16, is activated and promotes growth arrest in cells undergoing senescence (Stein et al., 1999; Roninson, 2003; Serrano, 2007). The proliferation blockage associated with senescence seems to be irreversible because few cells actually recover from prolonged up-regulation of tumor suppressors, such as p53, p21, and p16.

Chemotherapy-induced senescence has been reported with mechanistically distinct agents including DNA alkylators, antimetabolites, topoisomerase inhibitors, irradiation, and some microtubule stabilizers (Chang et al., 1999; Klein et al., 2005; Schmitt, 2007). Senescence is typically induced at low drug concentrations, whereas high concentrations produce overwhelming damage that favors apoptosis. For example, treatment of human hepatoma cells with a low concentration of the indirect DNA-damaging agent doxorubicin (<100 nM) induces senescence, eventually leading to mitotic catastrophe, whereas a high concentration (20 μM) leads to apoptosis (Eom et al., 2005). Considering the broad mechanisms of action of the anticancer agents causally involved in tumor cell senescence, it is surprising that in initial studies, clinically important inhibitors of tubulin polymerization, such as vinblastine and vincristine, were not observed to be potent inducers of senescence (Chang et al., 1999; Schmitt, 2007), even though one would hypothesize that kinetochore nonattachment recognized by mitotic spindle checkpoints might lead to senescence (Yamada and Gorbsky, 2006). It is interesting that recent work by Arthur et al. (2007) suggests that the inhibitor of tubulin polymerization, JG-03-14 (Arthur et al., 2007), caused senescence in residual surviving cell populations. Treatment of L929 mouse fibroblasts and PtK2 rat kangaroo kidney epithelial cells for 5 days with disorazole A_1 caused enlarged cells with increased metabolic activity that ceased to divide, possibly indicating that these surviving cells adopted a senescence phenotype (Elnakady et al., 2004). We found positive β-galactosidase staining in cells treated with disorazole C_1 at concentrations well below the IC_{50}. Prominent β-galactosidase staining was not observed previously with vinblastine (Lee et al., 2006), which no doubt contributed to the current belief that inhibition of microtubule polymerization does not provide a signal for senescence (Schmitt, 2007). We also did not observe significant β-galactosidase expression in cells treated with vinblastine or vincristine at their IC_{50} concentrations for growth inhibition. It is also important to note, however, that β-galactosidase expression has been questioned as a marker for senescence (Lee et al., 2006). Thus, we examined additional markers, including increased p53 and p21 with down-regulation in total Rb and phospho-Rb consistent with senescence. A549 cells do not express another common marker of senescence, $p16^{INK4}$; rather, they use p21 to maintain cell cycle arrest and senescence (Kashiwabara et al., 1998; McConnell et al., 1998). We saw increases in the levels of cyclin D, and the cyclin-dependent kinase inhibitor p21 was also elevated. It has been suggested that this phenomenon occurs because of hypermitogenic senescence, where supraphysiologic levels of mitogens (Ras/Raf/mitogen-activated protein kinase) increase cyclin D levels (Blagosklonny, 2003), but to date, our efforts to identify activation of the mitogen-activated protein kinase pathway have not been successful. Finally, another marker of senescence is inhibition of DNA synthesis, which was markedly decreased in cells exposed to disorazole C_1 as early as 24 h after treatment with low concentrations (≥0.5 nM); both discodermolide and vinblastine were less efficacious.

In summary, our data provide evidence that microtubule destabilization can suppress cancer cell growth by inducing premature senescence at concentrations at or below the IC_{50} for growth inhibition. Other microtubule-destabilizing agents, namely JG-03-14, also are reported to cause premature senescence (Arthur et al., 2007), albeit at higher concentrations (namely 500 nM, which causes 70–80% growth inhibition) than that required with disorazole C_1. These results illustrate that microtubule disruption, like some other forms of cellular stress, provided intracellular signals promoting premature senescence, at least in some tumor cell types. The propensity of disorazole C_1 to promote senescence may be related to the prolonged cellular effects or the nature of its interactions with microtubules. The symmetric synthesis of disorazole C_1 (Wipf and Graham, 2004; Wipf et al., 2006) enables the production of radiolabeled compound and analog development. We speculate that disorazole C_1 could be a potent and valuable chemical probe for studying the process of premature senescence induced by mitotic spindle disruption.

Acknowledgments

We thank Drs. Jennifer Grandis (University of Pittsburgh) and June Biedler (Memorial Sloan-Kettering Cancer Center, New York, NY) for providing the head and neck carcinoma and Chinese hamster lung cell lines, respectively; Drs. Kenneth Bair and Fred Kinder at Novartis for providing the discodermolide; and Dr. Eckhard Günther at Æterna Zentaris for providing disorazole A_1.

References

Arthur CR, Gupton JT, Kellogg GE, Yeudall WA, Cabot MC, Newsham IF, and Gewirtz DA (2007) Autophagic cell death, polyploidy and senescence induced in breast tumor cells by the substituted pyrrole JG-03-14, a novel microtubule poison. *Biochem Pharm* **74:**981–991.

Bai R, Taylor GF, Cichacz ZA, Herald CL, Kepler JA, Pettit GR, and Hamel E (1995a) The spongistatins, potently cytotoxic inhibitors of tubulin polymerization, bind in a distinct region of the vinca domain. *Biochemistry* **34:**9714–9721.

Bai R, Taylor GF, Schmidt JM, Williams MD, Kepler JA, Pettit GR, and Hamel E (1995b) Interaction of dolastatin 10 with tubulin: induction of aggregation and binding and dissociation reactions. *Mol Pharmacol* **47:**965–976.

Blagosklonny MV (2003) Cell senescence and hypermitogenic arrest. *EMBO Rep* **4:**358–362.

Chang BD, Broude EV, Dokmanovic M, Zhu H, Ruth A, Xuan Y, Kandel ES, Lausch E, Christov K, and Roninson IB (1999) A senescence-like phenotype distinguishes tumor cells that undergo terminal proliferation arrest after exposure to anticancer agents. *Cancer Res* **59:**3761–3767.

Dimri GP, Lee X, Basile G, Acosta M, Scott G, Roskelley C, Medrano EE, Linskens M, Rubelj I, and Pereira-Smith O (1995) A biomarker that identifies senescent human cells in culture and in aging skin in vivo. *Proc Natl Acad Sci U S A* **92:**9363–9367.

Elnakady YA, Sasse F, Lünsdorf H, and Reichenbach H (2004) Disorazol A1, a highly effective antimitotic agent acting on tubulin polymerization and inducing apoptosis in mammalian cells. *Biochem Pharmacol* **67:**927–935.

Eom YW, Kim MA, Park SS, Goo MJ, Kwon HJ, Sohn S, Kim WH, Yoon G, and Choi KS (2005) Two distinct modes of cell death induced by doxorubicin:apoptosis and

cell death through mitotic catastrophe accompanied by senescence-like phenotype. *Oncogene* **24:**4765–4777.
Hamel E and Lin CM (1984) Separation of active tubulin and microtubule-associated proteins by ultra centrifugation and isolation of a component causing the formation of microtubule bundles. *Biochemistry* **23:**4173–4184.
Jansen R, Irschik H, Reichenbach H, Wray V, and Hofle G (1994) Disorazoles, highly cytotoxic metabolites from the sorangicin producing bacterium *Sorangium cellulosum*, strain So ce1. *Liebigs Ann Chem* 759–773.
Jordan MA and Wilson L (2004) Microtubules as a target for anticancer drugs. *Nat Rev Cancer* **4:**253–265.
Kashiwabara K, Oyama T, Sano T, Fukuda T, and Nakajima T (1998) Correlation between methylation status of the p16/CDKN2 gene and the expression of p16 and Rb proteins in primary nonsmall cell lung cancers. *Int J Cancer* **79:**215–220.
Klein LE, Freeze BS, Smith AB 3rd, and Horwitz SB (2005) The microtubule stabilizing agent discodermolide is a potent inducer of accelerated cell senescence. *Cell Cycle* **4:**501–507.
Kopp M, Irschik H, Pradella S, and Müller R (2005) Production of the tubulin destabilizer disorazol in *Sorangium cellulosum*: biosynthetic machinery and regulatory genes. *Chembiochem* **6:**1277–1286.
Lee BY, Han JA, Im JS, Morrone A, Johung K, Goodwin EC, Kleijer WJ, DiMaio D, and Hwang ES (2006) Senescence-associated beta-galactosidase is lysosomal beta-galactosidase. *Aging Cell* **5:**187–195.
McConnell BB, Starborg M, Brookes S, and Peters G (1998) Inhibitors of cyclin-dependent kinases induce features of replicative senescence in early passage human diploid fibroblasts. *Curr Biol* **8:**351–354.
Roninson IB (2003) Tumor cell senescence in cancer treatment. *Cancer Res* **63:**2705–2715.
Schmitt CA (2007) Cellular senescence and cancer treatment. *Biochim Biophys Acta* **1775:**5–20.
Serrano M (2007) Cancer regression by senescence. *New Engl J Med* **356:**1996–1997.
Stein GH, Drullinger LF, Soulard A, and Dulić V (1999) Differential roles for cyclin-dependent kinase inhibitors p21 and p16 in the mechanisms of senescence and differentiation in human fibroblasts. *Mol Cell Biol* **19:**2109–2117.
Stout JR, Rizk RS, Kline SL, and Walczak CE (2006) Deciphering protein function during mitosis in PtK cells using RNAi. *BMC Cell Biol* **7:**26.
Tierno MB, Petrik B, Nickischer D, and Johnston P Application Note LC01612000, Thermo Scientific.
Wang Z, McPherson PA, Raccor BS, Balachandran R, Zhu G, Day BW, Vogt A, and Wipf P (2007) Structure-activity and high-content imaging analyses of novel tubulysins. *Chem Biol Drug Des* **70:**75–86.
Wipf P and Graham TH (2004) Total synthesis of (-)-disorazole C1. *J Am Chem Soc* **126:**15346–15347.
Wipf P, Graham TH, Vogt A, Sikorski RP, Ducruet AP, and Lazo JS (2006) Cellular analysis of disorazole C and structure-activity relationship of analogs of the natural product. *Chem Biol Drug Des* **67:**66–73.
Yamada HY and Gorbsky GJ (2006) Spindle checkpoint function and cellular sensitivity to antimitotic drugs. *Mol Cancer Ther* **5:**2963–2969.

Address correspondence to: John S. Lazo, Department of Pharmacology and Chemical Biology, University of Pittsburgh Drug Discovery Institute, Biomedical Science Tower 3, Suite 10040, 3401 Fifth Avenue, University of Pittsburgh, Pittsburgh, PA 15260. E-mail: lazo@pitt.edu